PCCP

Accepted Manuscript

This is an *Accepted Manuscript*, which has been through the Royal Society of Chemistry peer review process and has been accepted for publication.

Accepted Manuscripts are published online shortly after acceptance, before technical editing, formatting and proof reading. Using this free service, authors can make their results available to the community, in citable form, before we publish the edited article. We will replace this *Accepted Manuscript* with the edited and formatted *Advance Article* as soon as it is available.

You can find more information about *Accepted Manuscripts* in the **Information for Authors**.

Please note that technical editing may introduce minor changes to the text and/or graphics, which may alter content. The journal's standard **Terms & Conditions** and the **Ethical guidelines** still apply. In no event shall the Royal Society of Chemistry be held responsible for any errors or omissions in this *Accepted Manuscript* or any consequences arising from the use of any information it contains.

Automatic Mechanism Generation for Pyrolysis of Di-*tert*-butyl Sulfide

Caleb A. Class[a,b], Mengjie Liu[a], Aäron G. Vandeputte[a,c], William H. Green[a,d]

Abstract

The automated Reaction Mechanism Generator (RMG), using rate parameters derived from ab initio CCSD(T) calculations, is used to build reaction networks for the thermal decomposition of di-tert-butyl sulfide. Simulation results were compared with data from pyrolysis experiments with and without the addition of a cyclohexene inhibitor. Purely free-radical chemistry did not properly explain the reactivity of di-tert-butyl sulfide, as the previous experimental work showed that the sulfide decomposed via first-order kinetics in the presence and absence of the radical inhibitor. The concerted unimolecular decomposition of di-tert-butyl sulfide to form isobutene and tert-butyl thiol was found to be a key reaction in both cases, as it explained the first-order sulfide decomposition. The computer-generated kinetic model predictions quantitatively match most of the experimental data, but the model is apparently missing pathways for radical-induced decomposition of thiols to form elemental sulfur. Cyclohexene has a significant effect on the composition of the radical pool, and this led to dramatic changes in the resulting product distribution.

Introduction

Sulfur compounds are important in many aspects of life, including food, fuels, and the environment.[1–3] Sulfur in fuel sources can lead to problems in processing and usage. Sulfur in crude oil leads to some challenges, as a sufficient amount of these compounds must be removed during refinement to satisfy governmental regulations and prevent the release of toxic sulfur compounds into the environment and the poisoning of catalytic converters.[4–6] In pyrolysis and steam cracking, sulfur compounds have a significant impact on the initiation, termination, and product distribution[7], leading to undesired process variability.

Because of the importance of these compounds, significant experimental efforts have been undertaken to understand their chemistry, from pyrolysis[8–10] to oxidation[11,12] to decomposition in aqueous and

supercritical environments.[13–16] Due to the complexity in building accurate mechanisms to model these phenomena, most of the available literature on sulfur chemistry includes only speculative mechanisms without quantitative product predictions. However, some detailed mechanisms have been developed for small sulfides. Vandeputte et al. studied dimethyl disulfide decomposition computationally and proposed a mechanism with satisfactory agreement with experiment.[17] Zheng et al. have studied pyrolysis and oxidation of diethyl disulfide experimentally and computationally, and have proposed a detailed mechanism.[18,19]

The development of automated reaction mechanism generation software[20,21] has greatly aided in the effort to understand sulfur chemistry. Recently, Van de Vijver et al. have successfully used the automated kinetic model builder Genesys to build mechanisms for thermal decomposition of diethyl sulfide and ethyl methyl sulfide.[22] The automated mechanism builder used in the present work, Reaction Mechanism Generator (RMG), has been successfully used to develop mechanisms for many systems,[23–26] but has thus far been largely limited to the study of C/H/O chemistry without sulfur. As demonstrated here, with extensions to the software and the availability of improved estimation methods for the thermochemistry and reaction rates of elementary organosulfur reactions,[27–29] it is now possible to use this computational tool to shed mechanistic insight on experimental studies of sulfur chemistry.

Martin et al. previously studied the pyrolysis of a variety of alkyl tert-butyl sulfides,[30] and most of the observed product distributions supported the four-centered transition state suggested by Benson and Haugen,[31] which is presented in Figure 1. Di-tert-butyl sulfide,[8] which was pyrolyzed between 360 and 413 °C with and without the presence of a supposed radical inhibitor, cyclohexene, was the main exception to the trend. The expected products of the four-center reaction were observed in the presence of cyclohexene, but significantly different product distributions were obtained in the case of neat pyrolysis. In this work, quantum chemistry calculations and kinetic mechanisms built by RMG are used to clarify the key reaction steps for the two cases.
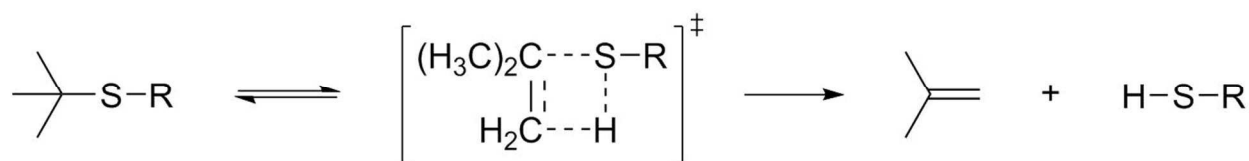

Figure 1. Proposed reaction pathway for the decomposition of an alkyl tert-butyl sulfide.[31]

Methods

The new Python version of RMG was used to generate the mechanisms for this work.[21,32] RMG uses an iterative, flux-based algorithm to build reaction mechanisms. With a user-supplied set of initial "core" species, RMG searches a database containing a set of specific reactions and a more general library of reaction recipes, to determine all possible reactions for the given species. The products of these reactions are then added to the model's "edge" if they are not already present in the mechanism. The reaction mixture is then simulated with the user-specified conditions and initial concentrations, until an edge species reaches the required flux to be added into the core. This required flux is defined as a fraction of the characteristic flux of all of the reactants currently in the core (the fraction is provided by the user as the "move-to-core tolerance".[21] The database is then searched for reactions of the newly expanded core. The whole process repeats until the specified termination condition is reached without any of the edge species being formed at a significant rate, as defined above. The final mechanism only contains the core species and reactions, and this is output as a CHEMKIN input file.[33]

Two models were generated for this work, corresponding to the reactant mixtures and conditions of the experiments by Martin and Barroeta:[8] One was built for pyrolysis of neat di-tert-butyl sulfide, and one for pyrolysis of a mixture of 40 mole% di-tert-butyl sulfide and 60 mole% cyclohexene. The RMG simulations were conducted for a reactor at a temperature of 380 °C and a pressure range of 15-217 Torr. Given the relatively low temperature conditions, high-pressure-limit rate parameters were used. A goal reactant conversion of 60% was used for both cases, with a move-to-core tolerance of 0.05 for the neat pyrolysis model and 0.01 for the cyclohexene model. We were unable to verify the convergence of the neat pyrolysis model with respect to the tolerance, as the RMG simulation could not be run to completion with tighter tolerances. For the cyclohexene model, we confirmed convergence with respect to the tolerance, as tighter tolerances gave the same result. The resulting CHEMKIN input file was used to simulate the reactions at the experimental conditions used by Martin and Barroeta.[8]

Thermochemical parameters were calculated using the group additivity values developed by Vandeputte et al.[29] Kinetic parameters from the RMG database[34] were used to estimate reaction rate constants. The database contains rate parameters for organosulfur reactions, including hydrogen abstraction,[28,35,36] beta-scission,[37] and homolytic substitution reactions,[38] most of which were computed at the CBS-QB3 level of theory using transition state theory.

Reactions found to be of particular importance in the model predictions were refined further by calculating single-point energies at the CCSD(T)-F12a/cc-pVDZ-F12 level of theory after geometry

optimizations, scaled (0.99) harmonic frequency calculations, and hindered rotor scans using B3LYP/6-311G(2d,d,p). As shown by Aguilera-Iparraguirre and co-workers, enthalpies computed using CCSD(T)-F12a/cc-pVDZ-F12 typically agree within 2 kJ/mole with those computed using CCSD(T)-F12a/cc-pVTZ-F12,[39-42] so we estimate that they are within about 4 kJ/mole of the basis-set limit. While CCSD(T) is a very good quantum chemistry method, it is not perfect, and the geometries, frequencies, and hindered rotor calculations based on DFT calculations also introduce some uncertainty, so we estimate the true uncertainties in computed enthalpies and barrier heights are about 10 kJ/mole. A double-zeta basis set was chosen for this work because of the relatively large systems under consideration, which contain up to 10 heavy atoms.

After quantum calculations were completed in Gaussian 03[39] and Molpro,[40] the open-source CanTherm software package[41] was used to calculate TST rate constants between 300 and 2000 K, including hindered rotor corrections and a tunneling correction using the Eckart method.[42] The rate constants were then fit to the modified Arrhenius form,

$$k(T) = AT^n \exp\left(\frac{-E_a}{RT}\right)$$

where T is the temperature in Kelvin, R is the gas constant, A and n are fitted constants, and E_a is the fitted activation energy, which is different from the zero-point-energy corrected reaction energy barrier ΔE_0. The full reaction mechanisms and all of the computed values are detailed in the Supporting Information.

Results and Discussion

Unimolecular or Radical Decomposition Mechanism

To better understand the decomposition of di-tert-butyl monosulfide, it may also be useful to consider the mechanism of the corresponding disulfide. Martin and Barroeta proposed a set of unimolecular reactions for the decomposition of di-tert-butyl disulfide to explain the formation of isobutene and hydrogen disulfide from the initial reactant, but these steps remained speculative and based on their experimental results.[43] We found transition states using quantum chemistry methods for the unimolecular decompositions of di-tert-butyl disulfide and tert-butyl hydrodisulfide, and their geometries can be seen in Figure 2. The analogous mechanism is also possible in the pyrolysis of di-tert-butyl monosulfide, and optimized transition states for these reactions are presented in Figure 3.
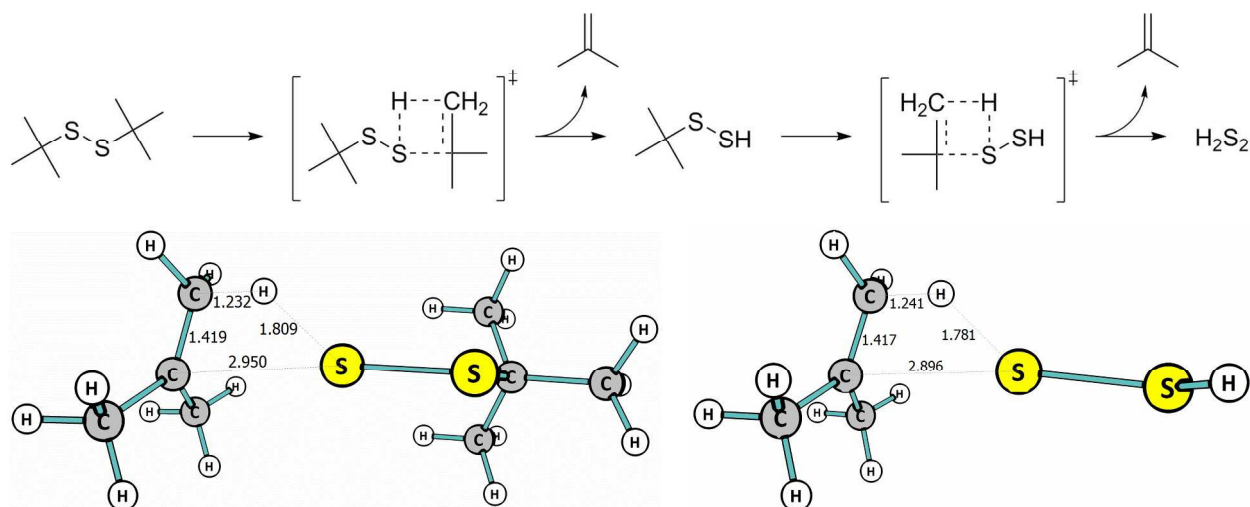
Figure 2. Proposed reaction pathway[39] (top) and optimized transition state geometries (bottom) for the molecular decomposition of di-tert-butyl disulfide. Distances (Å).
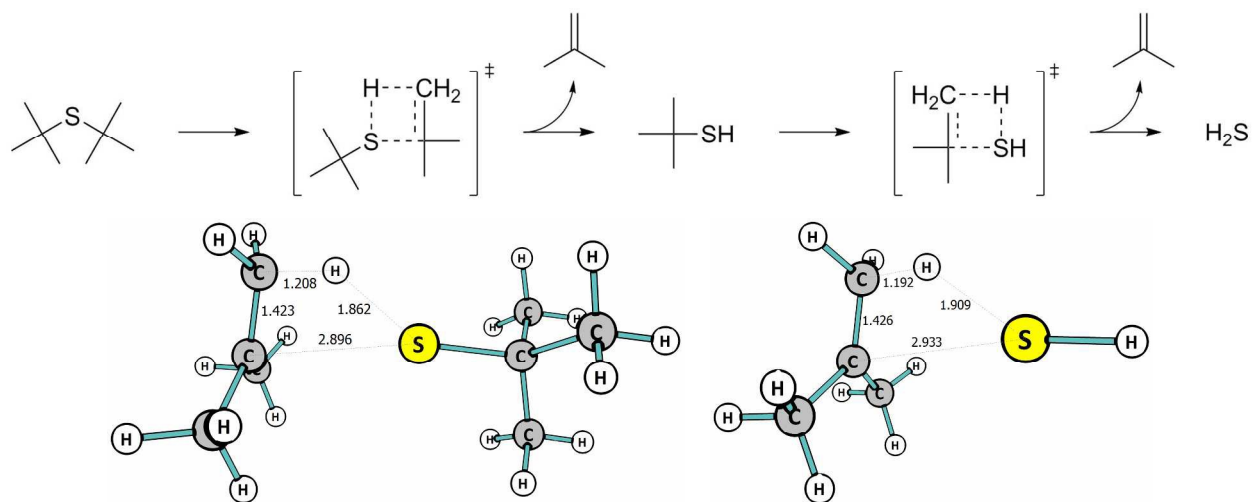

Figure 3. Proposed reaction pathway (top) and optimized transition state geometries (bottom) for the molecular decomposition of di-tert-butyl monosulfide. Distances (Å).

Table 1. Calculated rate constants (using CCSD(T)-F12/cc-pVDZ-F12) for molecular elimination reactions. A [s^{-1}], n [unitless], E_a [kJ/mol], k [s^{-1}].

			$\log_{10}A$	n	E_a	k (380 °C)
(1)			12.91	1.04	214.5	4.7×10^{-2}
(2)			13.66	0.39	233.8	1.2×10^{-4}
(3)			13.77	0.89	239.4	1.4×10^{-3}
(4)			13.83	0.36	256.0	2.3×10^{-6}

The calculated rate parameters are presented in Table 1. The activation energies in the disulfide mechanism (the first two reactions) are about 25 kJ/mol lower than their respective reactions in monosulfide decomposition, while the initial decomposition step of each mechanism, reactions (1) and (3), are entropically favored over subsequent reactions (2) and (4). While the calculated unimolecular rate constant for reaction (3) falls within the experimental uncertainty of the overall rate constant measured for di-tert-butyl monosulfide consumption,[8] the calculated rate for reaction (1) is an order of magnitude slower than the total disulfide consumption rate observed experimentally.[43] Calculations using a larger basis set might bring this prediction closer to the observation.

However, it is also likely that there is an additional free radical pathway which also contributes to the total consumption rate while resulting in the same major products. The RMG database predicts C—S and S—S bond breaking to occur at roughly the same rate in the disulfide, at about one order of magnitude slower than the initial unimolecular decomposition reaction. The RMG database estimates an energy of 284 kJ/mol and rate of 1.9×10^{-4} s^{-1} for S—S bond breaking, and a bond energy of 243 kJ/mol and rate of 1.3×10^{-4} s^{-1} for C—S breaking in the disulfide. These reactions, and the ensuing propagation steps, will provide an appreciable amount of the disulfide decomposition.

The overall trend in Table 1 provides some insight into the differences between the reaction mechanisms of di-tert-butyl monosulfide and di-tert-butyl disulfide. While di-tert-butyl disulfide undergoes the full molecular mechanism (with some contribution from the radical mechanism) to form isobutene and hydrogen disulfide—some of which can react further to form hydrogen sulfide—the elimination of H_2S from tert-butyl thiol is slower than the other three reactions in Table 1 by two or more orders of magnitude, due to a higher activation energy and lower activation entropy. This suggests that the consumption of tert-butyl thiol may occur more quickly by a free-radical mechanism. This would explain the equal consumption rate of di-tert-butyl monosulfide with and without the radical inhibitor, with the cyclohexene inhibiting the radical pathway for H_2S formation from tert-butyl thiol. The exact mechanism can be explored in more detail using RMG.

Neat Pyrolysis of di-*tert*-Butyl Sulfide

For the neat pyrolysis system, RMG generated a mechanism with 147 species and 996 reactions. The full mechanism including thermodynamic and kinetic parameters is included in the Supplementary Information in CHEMKIN format. The main reaction pathways are presented in Figure 4, with major products in boxes and intermediate products, which continue to form a variety of other minor products,

in dashed boxes. Pathway (a), homolytic scission of a C—S bond, accounts for an appreciable amount (12%) of the overall sulfide decomposition, and it provides most of the predicted isobutane production. This reaction occurs much quicker than analogous bond-scissions of other hydrocarbons due to the weakness of the C—S single-bond; this one is particularly fast due to the production of a tertiary tert-butyl radical in addition to the thiyl compound.

Pathways (b) and (c) provide the majority of the main product, isobutene. Pathway (b), which starts with the molecular elimination reaction that directly forms tert-butyl thiol and isobutene, is predicted to account for 78% of sulfide conversion. This is a sensible result based on the experimental data, as this reaction would explain the overall first-order consumption of di-tert-butyl sulfide observed in the presence and absence of cyclohexene. Much of the thiol undergoes abstraction of the hydrogen bonded to the sulfur to form a thiyl radical. This radical is also produced in smaller amounts through pathway (c), which requires hydrogen abstraction from one of the six methyl groups on di-tert-butyl sulfide, prior to a beta-scission reaction that also forms isobutene. The tert-butyl thiyl radical undergoes intramolecular hydrogen abstraction from one of its own methyl groups, and the resulting radical species undergoes beta-scission to form the HS radical, which then abstracts hydrogen to form hydrogen sulfide.

Comparisons between the experimental data and RMG predictions are presented in Figure 5 and Figure 6. Martin and Barroeta used the C_4 yield as a measure of reactant conversion, and calculated it based on the amount of carbon in the measured products.[8] Here, we used the ratio of the product partial pressures to the initial reactant partial pressure to define C_4 yield:

$$C_4 \text{ Yield } (\%) = \frac{p_{C4H8} + p_{C4H10} + p_{C4H9SH}}{2 \times p_{DTBS,i}} \times 100$$

These plots show excellent agreement between model and experimental data, as C_4 yield is predicted within 10% of the experimental observation and the predicted pressure increase also matches very well. However, tert-butyl thiol is notably overpredicted. The experiments noted production of a yellow solid during pyrolysis, which was assumed to be elemental sulfur, primarily S_8. Apparently, there is a process which converts most of the thiol to isobutane and sulfur on a timescale of approximately 20 minutes. However, the current model is missing pathways for S_8 formation, as speculative pathways failed to predict appreciable formation of this product. Thus, the discrepancy in the thiol prediction is likely a result of the lack of this desulfurization pathway.
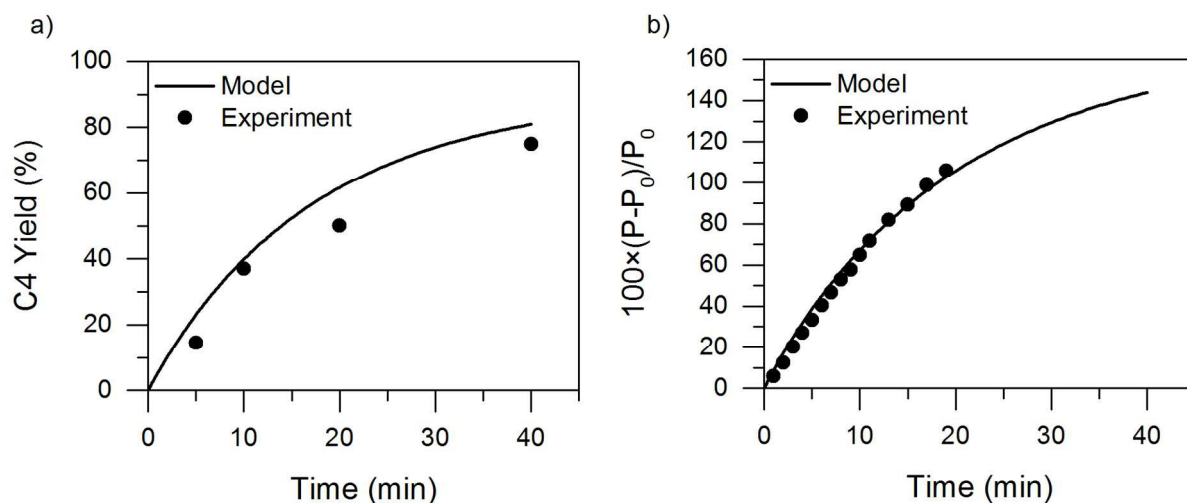
Figure 4. Major reaction pathways for neat pyrolysis of di-tert-butyl sulfide at 380 °C. Percentages represent total proportion of reacted sulfide proceeding through a pathway over 40 minutes, rounded to nearest percent. Pathways comprising less than 1% are not shown.

Figure 5. Experimental[8] and simulated results for a) C_4 yield from neat di-tert-butyl sulfide at 380 °C, and b) pressure increase at same conditions.
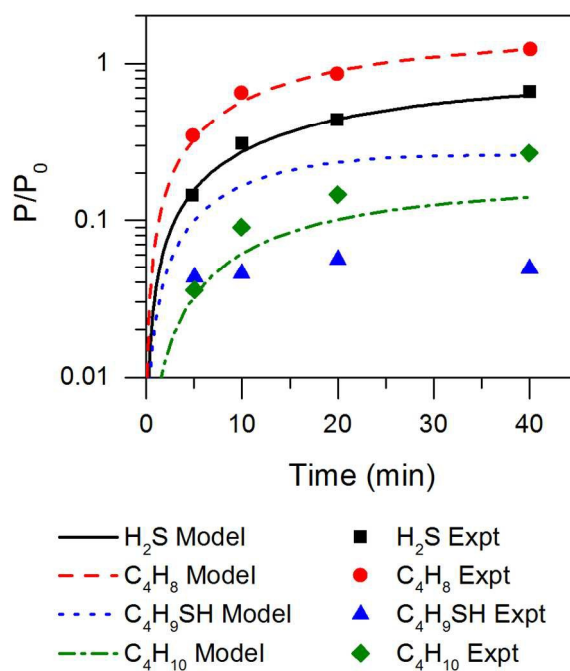

Figure 6. Experimental[8] and simulated results for major products of neat di-tert-butyl sulfide pyrolysis, presented in logarithmic scale as a fraction of initial reactant concentration.

Pyrolysis of di-tert-butyl sulfide with Cyclohexene

The final mechanism from the RMG simulation includes 69 species and 392 reactions, and the predicted overall fluxes over 40 minutes are presented in Figure 7. The same three major pathways are predicted as in the pyrolysis mechanism in the absence of cyclohexene. Again, the concerted reaction (b)

dominates, so we would expect sulfide decomposition to follow the same first-order kinetics (with roughly the same rate) as in the absence of the inhibitor, and this is what was observed experimentally.
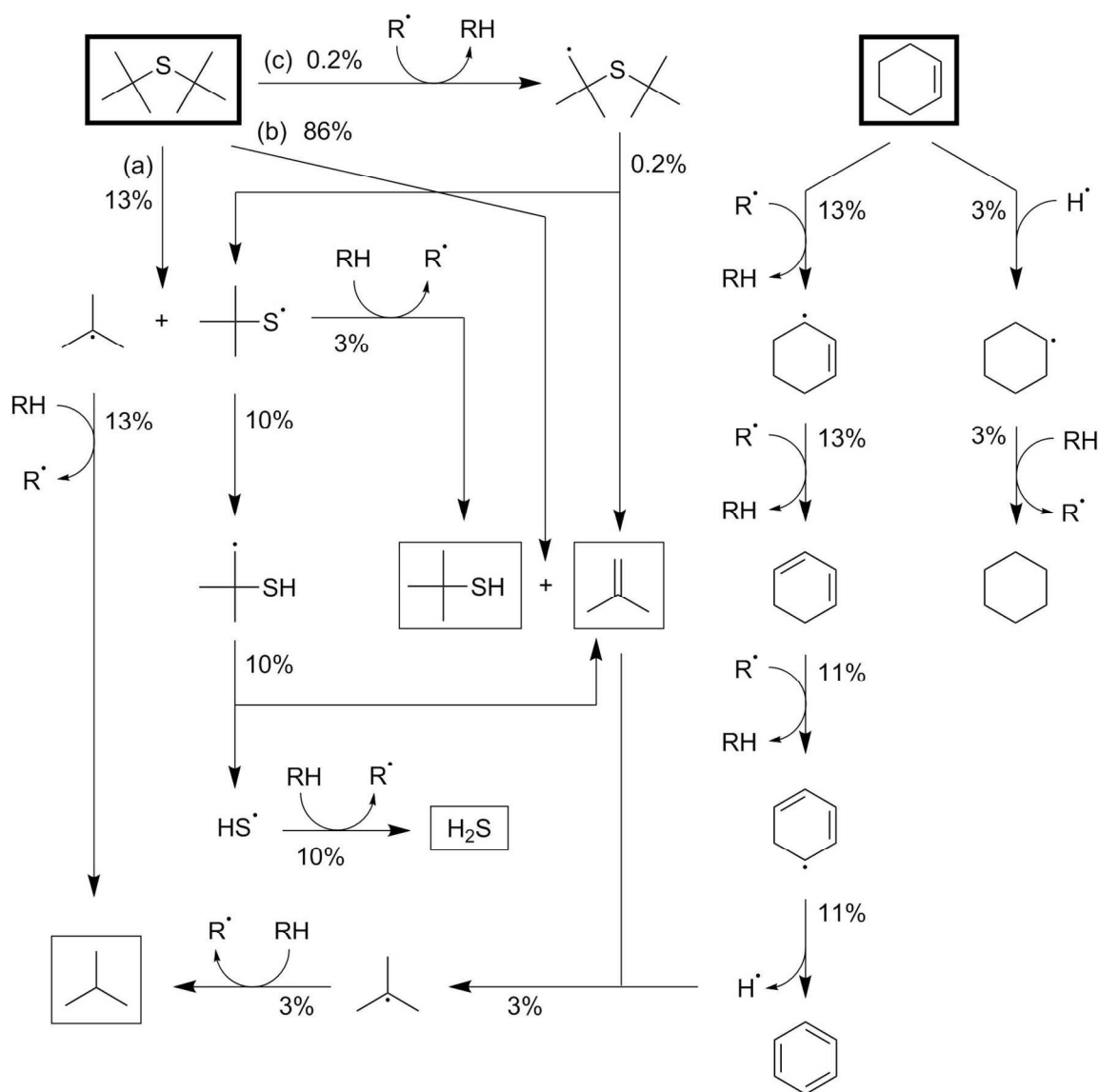

Figure 7. Major reaction pathways for pyrolysis of di-tert-butyl sulfide in the presence of cyclohexene at 380 °C. Percentages represent total proportion of reacted sulfide proceeding through a pathway over 40 minutes, rounded to nearest percent. Pathways comprising less than 1% are not shown.

The main difference between the predicted reaction mechanisms for the two cases is seen in the relative rate of pathway (c). Cyclohexene traps active radicals and readily donates hydrogen atoms to reverse reaction (c), causing the overall flux to be much lower. Cyclohexene also provides hydrogen in the production of H_2S and isobutane, resulting in a resonance-stabilized radical, which can further donate hydrogen atoms to eventually form a small amount of benzene. These compounds will also

donate hydrogen atoms to the thiyl radical produced through pathway (a), so instead of thiol producing thiyl, the process runs in reverse. Due to this prevention of the secondary decomposition of the thiol, this compound is predicted to have a concentration roughly equal to isobutene, consistent with the experiments.

A comparison of the experimental and predicted C_4 yield and reactor pressure increase is presented in Figure 8, and the product predictions are compared with experiments in Figure 9. C_4 yield and pressure increase are predicted with good accuracy, with the C_4 yield being within 25% of the experimental results. The pressure increase calculation neglects the initial pressure of cyclohexene, as was done by Martin and Barroeta.[8] Major products are also predicted reasonably accurately. The production of isobutane is underpredicted, and the overall C/H ratio of the C_4 products is larger than was observed experimentally, indicating that the net amount of hydrogens donated by cyclohexene is under-predicted by the model. The ratio of isobutane to isobutene is most sensitive to the two primary decomposition pathways of di-tert-butyl sulfide: molecular elimination and CS bond scission. The molecular pathway does not lead to significant hydrogen abstraction, while the radical pathway leads to two additional hydrogen abstraction steps which can increase the overall C/H ratio. Unfortunately, the experimental work did not report the yields for C6 and heavier products.

The large difference in the tert-butyl thiol yield between the inhibited and uninhibited cases suggests that the process to produce elemental sulfur is driven by active free radicals and so is quenched by cyclohexene. This is supported by the noted absence of solid sulfur produced in the experimental study.
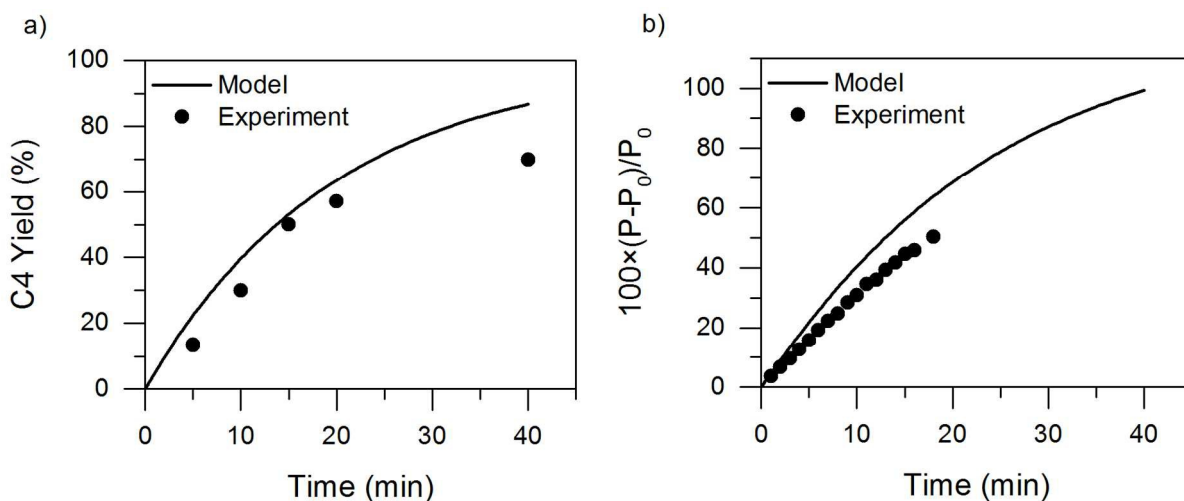

Figure 8. Experimental[8] and simulated results for a) conversion of di-tert-butyl sulfide in the presence of cyclohexene at 380 ℃, and b) pressure increase for same conditions.
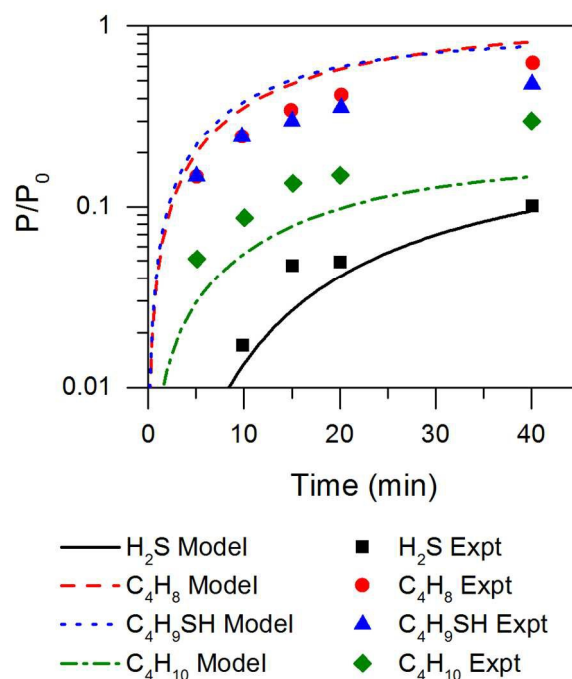
Figure 9. Experimental[8] and simulated results for products of di-tert-butyl sulfide pyrolysis in the presence of cyclohexene, presented in logarithmic scale as a fraction of initial sulfide concentration.

Mechanism Comparison

As seen in the previous section and in the experimental work, the addition of a cyclohexene inhibitor has little effect on the overall sulfide decomposition rate, as the dominating reaction for this process is the unimolecular decomposition reaction to form isobutene and tert-butyl thiol. This is further emphasized using sensitivity analysis, which shows this reaction as the most sensitive for sulfide decomposition by a wide margin. However, carbon-sulfur bond cleavage, which produces radicals, is only one order of magnitude slower, and the radical chemistry (which is strongly affected by the cyclohexene inhibitor) has a significant effect on the resulting product distributions. The major radical species concentrations are plotted in Fig. 10 for the two cases. While the total concentration of radical compounds is similar in the two cases, the presence of cyclohexene suppresses the concentration of radicals other than cyclohexenyl. The resonance-stabilized cyclohexenyl radicals abstract hydrogen more slowly than others, leading to slower radical-induced decompositions; this is particularly important for the thiol.
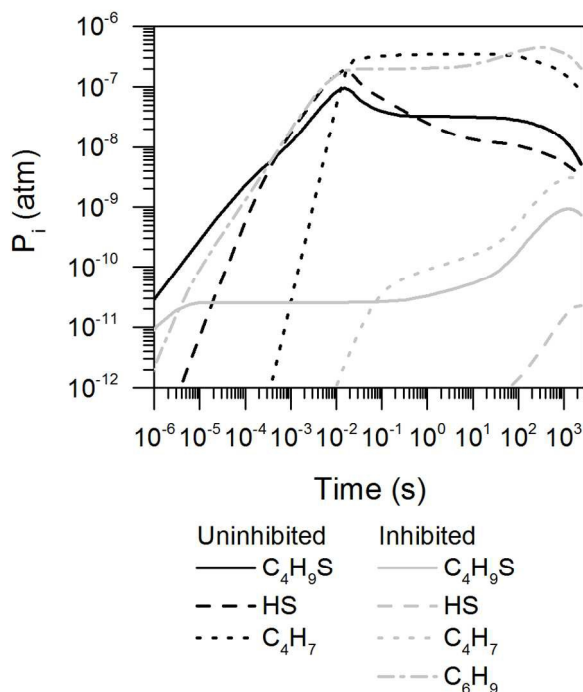
Figure 10. Major radical species present during pyrolysis of di-tert-butyl sulfide, with and without cyclohexene.

Conclusions

In this work, we have demonstrated the ability of automated mechanism generation software to propose and validate a detailed mechanism for pyrolysis of a tertiary sulfide. In particular, RMG was able to identify the most important reaction controlling the rate of di-tert-butyl sulfide decomposition in the presence and absence of a compound expected to inhibit the reaction rate. Coupled-cluster calculations suggested that the non-radical 4-center unimolecular decomposition pathway could almost fully account for the decomposition rate of di-tert-butyl sulfide. However, radical reactions have a significant effect on the product distribution. RMG was used to elucidate the reaction mechanism for di-tert-butyl sulfide, giving details on the important free radical pathways in the decomposition of tert-butyl thiol and explaining the drastic slowing of this decomposition pathway in the presence of the radical inhibitor, cyclohexene. The results obtained here suggest RMG may be a useful tool for understanding and predicting other organosulfur chemistry.

Acknowledgement

Notes and References

[a] Department of Chemical Engineering, Massachusetts Institute of Technology, Cambridge, MA 02139, USA. [b] Present Address: MD Anderson Cancer Center, Houston TX. [c] Present Address: SABIC, Elsloo, Netherlands. [d] whgreen@mit.edu

Bibliography

1.   Patai, S.; Rappoport, Z. The chemistry of sulphur-containing functional groups; Wiley, 1993; Vol. 102.
2.   Song, C. Catal. Today 2003, 86 (1-4), 211–263.
3.   Johnston, D. T. Earth-Science Rev. 2011, 106 (1-2), 161–183.
4.   Mohnen, V. A. Sci. Am. 1988, 259:2.
5.   Fishel, N. A.; Lee, R. K.; Wilhelm, F. C. Environ. Sci. Technol. 1974, 8 (3), 260–267.
6.   Corro, G. React. Kinet. Catal. Lett. 2002, 75 (1), 89–106.
7.   Bajus, M. Sulfur reports 1989, 9 (1), 25–66.
8.   Martin, G.; Barroeta, N. Int. J. Chem. Kinet. 1980, 12 (10), 699–716.
9.   Xu, L.; Yang, J.; Li, Y.; Liu, Z. Fuel Process. Technol. 2004, 85 (8-10), 1013–1024.
10. Winkler, J. K.; Karow, W.; Rademacher, P. J. Anal. Appl. Pyrolysis 2002, 62 (1), 123–141.
11. Timko, M. T.; Schmois, E.; Patwardhan, P. R.; Kida, Y.; Class, C. A.; Green, W. H.; Nelson, R. K.; Reddy, C. M. Energy & Fuels 2014, 28 (5), 2977–2983.
12. Mei, H.; Mei, B. W.; Yen, T. F. Fuel 2003, 82 (4), 405–414.
13. Katritzky, A. R.; Balasubramanian, M.; Siskin, M. Energy & Fuels 1992, 6 (4), 431–438.
14. Katritzky, A. R.; Barcock, R. A.; Balasubramanian, M.; Greenhill, J. V.; Siskin, M.; Olmstead, W. N. Energy & Fuels 1994, 8 (2), 498–506.
15. Kida, Y.; Class, C. A.; Concepcion, A. J.; Timko, M. T.; Green, W. H. Phys. Chem. Chem. Phys. 2014, 16 (20), 9220–9228.
16. Patwardhan, P. R.; Timko, M. T.; Class, C. a.; Bonomi, R. E.; Kida, Y.; Hernandez, H. H.; Tester, J. W.; Green, W. H. Energy and Fuels 2013, 27 (10), 6108–6117.
17. Vandeputte, A. G.; Reyniers, M.-F.; Marin, G. B. J. Phys. Chem. A 2010, 114 (39), 10531–10549.
18. Zheng, X.; Fisher, E. M.; Gouldin, F. C.; Zhu, L.; Bozzelli, J. W. Proc. Combust. Inst. 2009, 32 (1), 469–476.
19. Zheng, X.; Bozzelli, J. W.; Fisher, E. M.; Gouldin, F. C.; Zhu, L. Proc. Combust. Inst. 2011, 33 (1), 467–475.
20. Vandewiele, N. M.; Van Geem, K. M.; Reyniers, M.-F.; Marin, G. B. Chem. Eng. J. 2012, 207-208, 526–538.
21. Gao, C. W.; Allen, J. W.; Green, W. H.; West, R. H. Comput. Phys. Commun. 2016, 203, 212–225.
22. Van de Vijver, R.; Vandewiele, N. M.; Vandeputte, A. G.; Van Geem, K. M.; Reyniers, M.-F.; Green, W. H.; Marin, G. B. Chem. Eng. J. 2015, 278, 385–393.
23. Van Geem, K. M.; Reyniers, M.-F.; Marin, G. B.; Song, J.; Green, W. H.; Matheu, D. M. AIChE J. 2006, 52 (2), 718–730.

24.   Harper, M. R.; Van Geem, K. M.; Pyl, S. P.; Marin, G. B.; Green, W. H. Combust. Flame 2011, 158 (1), 16–41.
25.   Allen, J. W.; Scheer, A. M.; Gao, C. W.; Merchant, S. S.; Vasu, S. S.; Welz, O.; Savee, J. D.; Osborn, D. L.; Lee, C.; Vranckx, S.; Wang, Z.; Qi, F.; Fernandes, R. X.; Green, W. H.; Hadi, M. Z.; Taatjes, C. A. Combust. Flame 2014, 161 (3), 711–724.
26.   Gao, C. W.; Vandeputte, A. G.; Yee, N. W.; Green, W. H.; Bonomi, R. E.; Magoon, G. R.; Wong, H.-W.; Oluwole, O. O.; Lewis, D. K.; Vandewiele, N. M.; Van Geem, K. M. Combust. Flame 2015, 162 (8), 3115–3129.
27.   Vandeputte, A. G.; Reyniers, M.-F.; Marin, G. B. Theor. Chem. Acc. 2009, 123 (5-6), 391–412.
28.   Vandeputte, A. G.; Sabbe, M. K.; Reyniers, M.-F.; Marin, G. B. Phys. Chem. Chem. Phys. 2012, 14 (37), 12773–12793.
29.   Vandeputte, A. G.; Sabbe, M. K.; Reyniers, M.-F.; Marin, G. B. Chemistry 2011, 17 (27), 7656–7673.
30.   Martin, G. In *Sulphur-Containing Functional Groups (1993)*; John Wiley & Sons, Inc., 1993; pp 395–437.
31.   Benson, S. W.; Haugen, G. R. J. Am. Chem. Soc. 1965, 87 (18), 4036–4044.
32.   Green, W. H.; Allen, J. W.; Barlow, J.; Bhoorasingh, P. L.; Buesser, B. A.; Class, C. A.; Gao, C. W.; Han, K.; Seyedzadeh Khanshan, F.; Lambert, V.; Merchant, S. S.; Slakman, B. L.; Troiano, S.; Vandeputte, A. G.; Vandewiele, N. M.; West, R. H.; Yee, N. W. Reaction Mechanism Generator. http://reactionmechanismgenerator.github.io/.
33.   CHEMKIN-PRO 15131, 2013. CHEMKIN software is distributed by ANSYS.
34.   Green, W. H.; West, R. H.; RMG Team. RMG Database. https://github.com/ReactionMechanismGenerator/RMG-database.
35.   Vandeputte, A. G.; Reyniers, M.-F.; Marin, G. B. Chemphyschem 2013, 14 (16), 3751–3771.
36.   Vandeputte, A. G.; Sabbe, M. K.; Reyniers, M.-F.; Van Speybroeck, V.; Waroquier, M.; Marin, G. B. J. Phys. Chem. A 2007, 111 (46), 11771–11786.
37.   Vandeputte, A. G. The thermochemistry and decomposition mechanism of organosulfur and organophosphorus compounds, Ghent University, 2012.
38.   Vandeputte, A. G.; Reyniers, M.-F.; Marin, G. B. Chemphyschem 2013, 14 (8), 1703–1722.
39.   Frisch, M. J.; Trucks, G. W.; Schlegel, H. B.; Scuseria, G. E.; Robb, M. A.; Cheeseman, J. R.; Montgomery Jr., J. A.; Vreven, T.; Kudin, K. N.; Burant, J. C.; Millam, J. M.; Iyengar, S. S.; Tomasi, J.; Barone, V.; Mennucci, B.; Cossi, M.; Scalmani, G.; Rega, N.; Petersson, G. A.; Nakatsuji, H.; Hada, M.; Ehara, M.; Toyota, K.; Fukuda, R.; Hasegawa, J.; Ishida, M.; Nakajima, T.; Honda, Y.; Kitao, O.; Nakai, H.; Klene, M.; Li, X.; Knox, J. E.; Hratchian, H. P.; Cross, J. B.; Bakken, V.; Adamo, C.; Jaramillo, J.; Gomperts, R.; Stratmann, R. E.; Yazyev, O.; Austin, A. J.; Cammi, R.; Pomelli, C.; Ochterski, J. W.; Ayala, P. Y.; Morokuma, K.; Voth, G. A.; Salvador, P.; Dannenberg, J. J.; Zakrzewski, V. G.; Dapprich, S.; Daniels, A. D.; Strain, M. C.; Farkas, O.; Malick, D. K.; Rabuck, A. D.; Raghavachari, K.; Foresman, J. B.; Ortiz, J. V; Cui, Q.; Baboul, A. G.; Clifford, S.; Cioslowski, J.; Stefanov, B. B.; Liu, G.; Liashenko, A.; Piskorz, P.; Komaromi, I.; Martin, R. L.; Fox, D. J.; Keith, T.; Al-Laham, M. A.; Peng, C. Y.; Nanayakkara, A.; Challacombe, M.; Gill, P. M. W.; Johnson, B.; Chen, W.; Wong, M. W.; Gonzalez, C.; Pople, J. A. Gaussian 03, Revision D.01, 2004.
40.   Werner, H.-J.; Knowles, P. J.; Knizia, G.; Manby, F. R.; Schütz, M. Wiley Interdiscip. Rev. Comput. Mol. Sci. 2012, 2 (2), 242–253.
41.   Sharma, S.; Harper, M. R.; Green, W. H. CanTherm open-source software package. http://reactionmechanismgenerator.github.io/.
42.   Eckart, C. Phys. Rev. 1930, 35 (11), 1303–1309.
43.   Martin, G.; Barroeta, N. J. Chem. Soc. Perkin Trans. 2 1976, No. 12, 1421–1424.